Research article

Jiayi Wang, Zhuojun Liu*, Jin Xiang, Bo Chen, Yuming Wei, Wenjing Liu, Yi Xu, Sheng Lan and Jin Liu

Ultraviolet second harmonic generation from Mie-resonant lithium niobate nanospheres

https://doi.org/10.1515/nanoph-2021-0326
Received June 29, 2021; accepted August 25, 2021;
published online September 7, 2021

Abstract: Lithium niobate (LN), as a nonlinear material with a large nonlinear susceptibility, has been widely employed in second harmonic generation (SHG) up to ultraviolet (UV) frequency range due to its broad low-absorption window. In nanophotonics, it is possible to harness the Mie resonances associated with the single dielectric particles to boost the nonlinear light–matter interactions. Here, we fabricate single Mie-resonant LN nanospheres on a SiO_2 substrate via the femtosecond (fs) laser ablation technique. By exploiting the magnetic dipole (MD) Mie resonance, UV SHG from the LN nanosphere is significantly enhanced with a measured conversion efficiency of 4.45×10^{-8} under the excitation of an fs laser at 750 nm. The single LN nanospheres achieved in this work could serve as Mie resonators for building nonlinear nanophotonic devices such as frequency converters and quantum light sources, etc.

Keywords: lithium niobate; Mie resonance; nanosphere; second harmonic generation.

***Corresponding author**: **Zhuojun Liu**, State Key Laboratory of Optoelectronic Materials and Technologies, School of Physics, Sun Yat-sen University, Guangzhou 510275, China,
E-mail: liuzhj23@mail2.sysu.edu.cn. https://orcid.org/0000-0003-2063-8071
Jiayi Wang, **Bo Chen**, **Yuming Wei and Jin Liu**, State Key Laboratory of Optoelectronic Materials and Technologies, School of Physics, Sun Yat-sen University, Guangzhou 510275, China
Jin Xiang, Key Laboratory of Optoelectronic Technology and Systems, Ministry of Education, School of Optoelectronic Engineering, Chongqing University, Chongqing 400044, China. https://orcid.org/0000-0003-0896-7526
Wenjing Liu, State Key Laboratory for Mesoscopic Physics and Frontiers Science Center for Nano-optoelectronics, School of Physics, Peking University, 100871, Beijing, China
Yi Xu, Department of Electronic Engineering, College of Information Science and Technology, Jinan University, Guangzhou 510630, China
Sheng Lan, Guangdong Provincial Key Laboratory of Nanophotonic Functional Materials and Devices, School of Information and Optoelectronic Science and Engineering, South China Normal University, Guangzhou 510006, China

1 Introduction

As a fundamental optical nonlinear effect, second harmonic generation (SHG) is a process that two identical photons convert into a double-frequency photon, which has been widely applied in signal processing, optical spectroscopy, and laser systems [1–3]. Conventional SHG devices are based on bulk materials such as nonlinear crystals of potassium dihydrogen phosphate, potassium titanyl phosphate, and beta barium borate [4–9], where high-efficiency SHG requires phase-matching conditions and long interaction length with light. With the rapid developments of nanophotonics and integrated optics, building nanoscale nonlinear optical devices becomes feasible via the greatly enhanced light matter interactions provided by photonic nanostructures [10, 11]. Specifically, photonic microresonators that strongly enhance the local electromagnetic field can greatly boost the nonlinear optical processes [12, 13]. In addition, the tight confinement of light within sizes smaller than the coherent length of light eliminates the restriction of the phase-matching condition. One of the representative photonic nanostructures is single dielectric resonators such as nanospheres, nanocubes, and nanodisks that support Mie resonances [14–17]. With strong field confinement and great wavelength tunability by the size, geometry, and material composition, Mie resonators recently enable a wide range of applications in nonlinear nanophotonics such as Raman scattering [18, 19] and harmonic generations [19–21], as well as photon-pair generations [22, 23]. For most of these works, high refractive index dielectric materials with large nonlinear susceptibility such as silicon [24], gallium arsenide [25, 26], or germanium [27, 28] are employed, benefiting from their mature fabrication techniques and low loss in the near-infrared region. However, these materials are lossy in the ultraviolet (UV) range due to strong inter-band absorption, and therefore achieving strong UV SHG enhanced by Mie-resonant nanostructures remains an open challenge. Ferroelectric metal oxide lithium niobate (LN) with a large energy bandgap of 4 eV and a wide low-loss spectral

range from 0.33 to 5.5 μm [29–32] is a promising dielectric material for efficient SHG up to the UV region. Nevertheless, limited by the nanofabrication techniques, using LN single nanoparticles for nonlinear nanophotonics is not yet common. Recently, a high-efficiency SHG at 360 nm was demonstrated from Mie-resonant LN nanocubes fabricated by a solvothermal synthesis method [33]. However, bottom-up chemical synthesis is relatively complicated and the geometry of the Mie-resonators is limited to cubes. Alternatively, the femtosecond (fs) laser ablation technique has been successfully employed to fabricate Mie-resonant nanospheres with controllable size from a variety of nonlinear materials including Si, GaAs, Ge, and perovskite [34–37].

In this paper, we demonstrate a strong UV SHG from single LN nanospheres fabricated by the fs laser ablation technique. Supporting MD Mie resonance, LN nanospheres exhibit a significant field enhancement of 5.5, resulting in a high SHG conversion efficiency measured as 4.45×10^{-8}. We examine the wavelength and power dependence of the SHG signals, confirming the SHG enhancement contribution from the Mie resonance. Our work shows the feasibility of fabricating nanospheres from a bulk LN wafer and extends the Mie-resonance enhanced nanoscale SHG up to the UV frequency range.

2 Device design and fabrication

The schematic of SHG from a 160 nm-radius LN nanosphere placed on SiO_2 substrate is presented in Figure 1(a). A fs laser with wavelength of 750 nm is in resonance with the MD mode and the UV SH signal is expected to be at 375 nm. The scattering spectrum of the LN nanosphere is simulated via finite-difference time-domain (FDTD) method, which reveals the multipole contributions of the Mie resonances, as shown in Figure 1(b). We further calculate the Cartesian multipoles up to the third order based on the electric field E inside the structure. By using the multipolar expansion of the polarization current density [38], the multipole terms (electric dipole ED, magnetic dipole MD, electric quadrupole EQ, and magnetic quadrupole MQ) are calculated according to the following equations:

$$\mathrm{ED}_j = \frac{i}{\omega}\int J_j \mathrm{d}v \tag{1}$$

$$\mathrm{MD}_j = \frac{1}{2}\int (\boldsymbol{r}\times J)_j \mathrm{d}v \tag{2}$$

$$\mathrm{EQ}_{jk} = \frac{i}{\omega}\int \left(r_j J_k + r_k J_j - \frac{2}{3}\delta_{jk}(\boldsymbol{r}\cdot J)\right)\mathrm{d}v \tag{3}$$

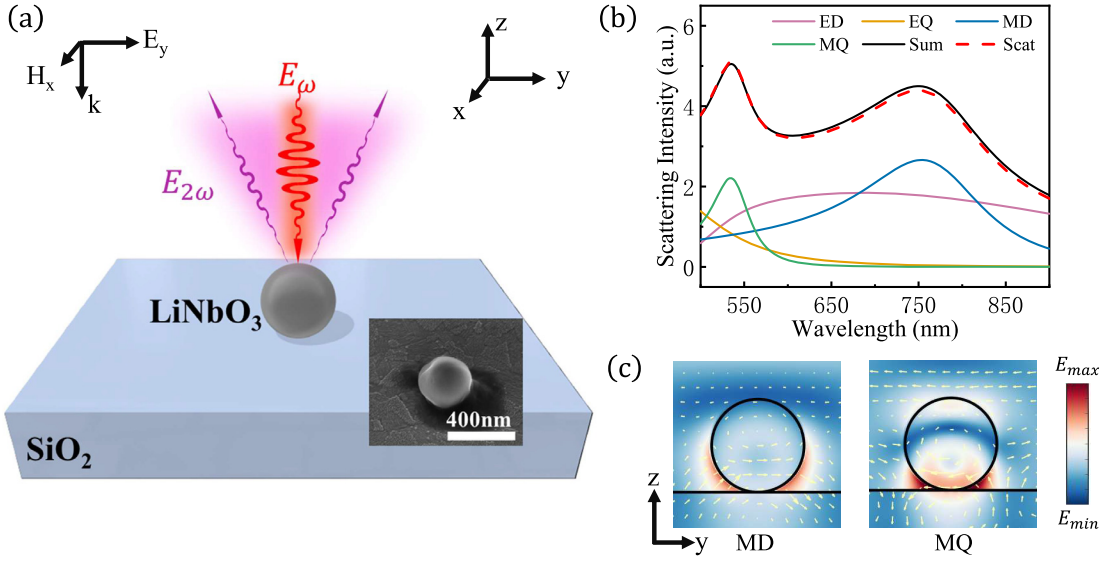

Figure 1: The design of LN nanosphere. (a) Schematic of ultraviolet SHG from an individual LN nanosphere on SiO_2 substrate. Inset: the SEM image of a fabricated nanosphere with a radius of 160 nm. (b) Simulated scattering spectra of an LN nanosphere. The calculated multipole contributions are depicted respectively with different colors (ED: electric dipole, EQ: electric quadrupole, MD: magnetic dipole, MQ: magnetic quadrupole.). (c) Electric field distribution of the Mie-resonant mode from an LN nanosphere at x–y plane, the white arrows indicate the in-plane electric field vectors.

$$\mathrm{MQ}_{jk} = \frac{1}{3}\int \left((\boldsymbol{r}\times\boldsymbol{J})_j r_k + (\boldsymbol{r}\times\boldsymbol{J})_k r_j\right) \mathrm{d}v \tag{4}$$

where ω is the angular frequency. The total scattered power P_{scat} is calculated as the sum of each multipole contributions:

$$\begin{aligned} P_{\mathrm{sact}} = {} & \frac{k^4\sqrt{\varepsilon_d}}{12\pi\varepsilon_0^2 c\mu_0}\left|\mathrm{ED}_j\right|^2 + \frac{k^4\varepsilon_d\sqrt{\varepsilon_d}}{12\pi\varepsilon_0 c}\left|\mathrm{MD}_j\right|^2 \\ & + \frac{k^6\varepsilon_d\sqrt{\varepsilon_d}}{160\pi\varepsilon_0^2 c\mu_0}\left|\mathrm{EQ}_{jk}\right|^2 + \frac{k^6\varepsilon_d^2\sqrt{\varepsilon_d}}{160\pi\varepsilon_0 c}\left|\mathrm{MQ}_{jk}\right|^2 \\ & + \frac{k^8\varepsilon_d^2\sqrt{\varepsilon_d}}{3780\pi\varepsilon_0^2 c\mu_0}\left|\mathrm{EO}_{jkl}\right|^2 + \frac{k^8\varepsilon_0^3\sqrt{\varepsilon_d}}{3780\pi\varepsilon_0 c}\left|\mathrm{MO}_{jkl}\right|^2 \end{aligned} \tag{5}$$

with k being the wave number and ε_0 is the vacuum permittivity, and ε_d is the relative permittivity of LN.

It can be observed that the two dominant peaks around 550 and 750 nm in the scattering spectrum are mostly attributed to the MQ and MD, respectively. In addition, the summation of individual multipole components strictly follows the simulated scattering spectrum via the FDTD method, which proves the reliability of the multipole decomposition. The simulated electric field distribution of the MD and MQ modes in the x-y plane of the LN nanosphere is shown in Figure 1(c). Inside the LN nanosphere, electric field enhancements are observed in both the MD and MQ modes. In this work, we choose to generate the SHG by pumping at the MD resonance simply because the SHG of the MQ mode is out of the detection range of our spectrometer.

We employ the fs laser ablation technique to fabricate LN nanospheres with radii ranging from 50 to 200 nm. In our experiments, 800 nm laser pulse with a temporal duration of 90 fs and repetition rate of 1 kHz are delivered by an fs amplifier (Legend Elite, Coherent) and then focused on the surface of an LN wafer immersed in deionized water. We use a lens with a focusing length of 15 cm to focus the laser beam on the LN wafer with a spot diameter of $\sim 70.0\mu$m. Once the ablation process is completed, the aqueous solution containing LN nanospheres is centrifuged with a speed of 6000 rpm to separate LN nanospheres with radii of 140–200 nm from small LN nanoparticles. Subsequently, the as-prepared LN nanospheres are randomly dispersed on a SiO_2 substrate with a low refractive index for effectively localizing the electromagnetic field. The scanning electron microscope (SEM) image of a fabricated LN nanosphere with a radius of 160 nm is shown in the inset of Figure 1(a). One of the advantages of our method is that the fabricated nanospheres can be flexibly transferred to any substrates due to their aqueous environment.

3 Results

A dark field spectroscopy setup has been implemented for measuring the scattering spectra of single LN nanospheres. The white light is focused onto individual nanospheres by a 100× darkfield objective, and the scattered light is collected by the same objective and delivered to an imaging spectrometer. To verify the Mie resonances associated with the LN nanospheres, the scattering spectra of LN nanospheres with different radii are simulated, as shown in Figure 2(a). With the increase of nanosphere radius, the MD-resonance wavelength redshifts significantly, following the relation $2R \approx \lambda/n$, where is the refractive index of the material, is the nanosphere radius, and is the Mie-resonant wavelength. Such a trend is in very good agreement with the measured spectra, as presented in Figure 2(b). The additional peak near 650 nm in the experiment possibly originates from the contribution of ED due to the deviation of the fabricated nanosphere from the ideal geometry.

The SHG signals are characterized by using an inverted microscope (Axio Observer A1, Zeiss) equipped with a spectrometer (SR-500i-B1, Andor) and a charge-coupled device (DU970N, Andor), as schematically shown in Figure 2(c). An fs laser oscillator with a pulse duration of 130 fs and repetition rate of 76 MHz (Mira 900S, Coherent) is used as the excitation source and a 100× objective lens (ZEISS Plan-Neofluar) is employed for signals collection. The backscattered incident laser beam is filtered by a short-pass filter (SPF, Thorlabs FES0450) so that the UV SHG signal can be collected by the spectrometer for analysis.

To investigate the nonlinear optical response of the LN nanospheres, SHG is measured from a 160 nm-radius nanosphere. With a pump power of 0.4 mW, SHG signals at different wavelengths are collected when scanning the pump laser across MD resonance (Figure 3(a)). The intensity of the SHG signal reaches the maximum at the MD resonance (750 nm) and significantly reduces at other pump wavelengths, implying the resonant enhancement from the MD mode. To further confirm the critical role played by the Mie resonance, the scattering spectrum of Mie-resonant mode and wavelength-dependent SHG intensities are plotted in Figure 3(b). It can be observed that the intensities of the SHG signals follow the profile of the scattering spectrum, clearly demonstrating that the enhancement of the nonlinear interactions is provided by the MD Mie resonance.

We examine the power dependence of the UV SHG from the LN nanosphere pumped at the MD Mie resonance. The measured SHG spectra under different pump powers are displayed in Figure 4(a). The SHG intensity as

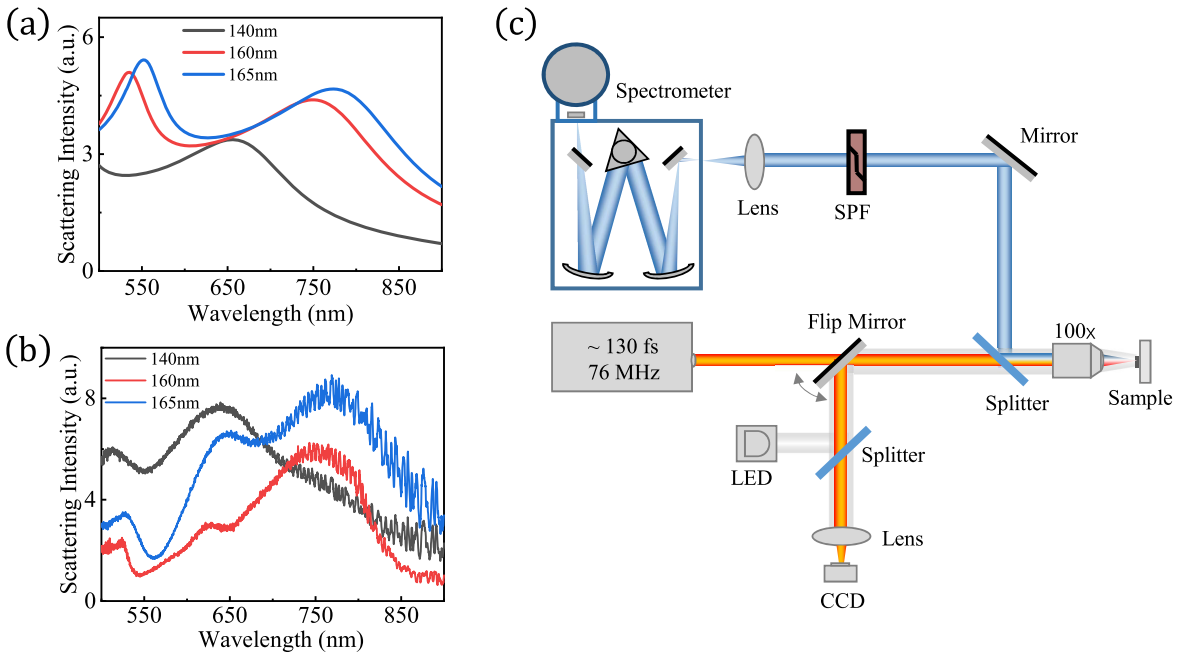

Figure 2: The characterization of the scattering spectra for LN nanosphere. (a) Simulated and (b) experimental scattering spectra of LN nanospheres with different radii. (c) Detection set up for collection of SHG signals from LN nanospheres. The fs incident laser beam is focused on the sample by an objective lens. The reflected incident laser is filtered by a short-pass filter (SPF) and then the backscattered SHG signal is collected by the spectrometer.

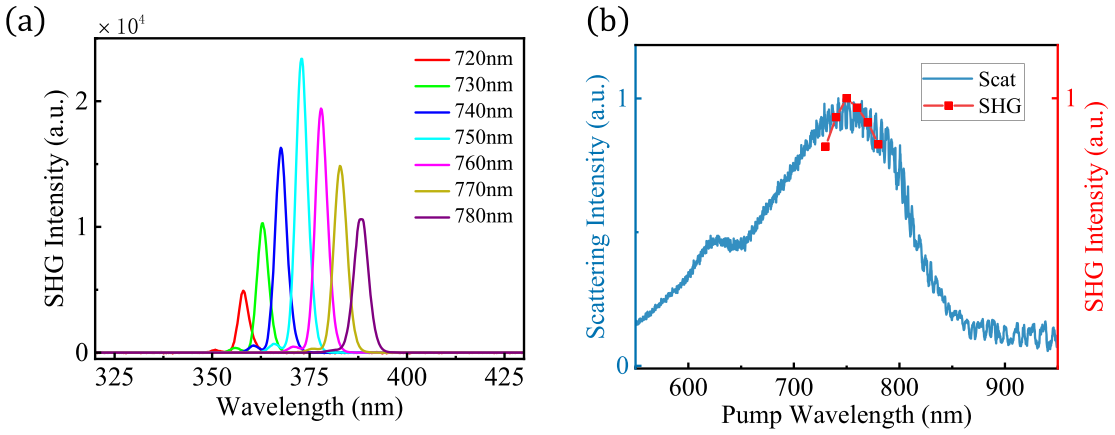

Figure 3: The characterization of the SHG enhancement for LN nanosphere. (a) Measured spectra of SHG when scanning the pump wavelength across MD mode under the pump power of 0.4 mW. (b) Wavelength dependence of SHG signals in (a). The scattering spectrum of the corresponding LN nanosphere is plotted for comparison.

a function of the pump power is plotted in Figure 4(b) in a double logarithmic scale, exhibiting an exponent value of 2.0 by fitting with $P_{\mathrm{SHG}} = mP^{n}_{\mathrm{pump}}$. The strict quadratic dependence of the signal intensity on the pump power unequivocally verifies the nature of the second-order nonlinear optical process. Finally, with an incident peak irradiance of 2.0 GW/cm^2, the maximal measured efficiency of visible-to-UV conversion is extracted as high as 4.45×10^{-8} from the equation $\eta = P_{2\omega}/P_{\omega}$, which is comparable to the previous works on LN metasurfaces [39, 40]. We note that the SiO_2 substrate used in this work results in low-Q factors and weaker field enhancements for the MD Mie-resonances compared to the situation without a substrate. The SHG conversion efficiency can be further improved by engineering the substrate. E.g., replacing the SiO_2 substrate with hyperbolic metamaterials has been suggested to generate high-efficiency SHG from single LN particles [41].

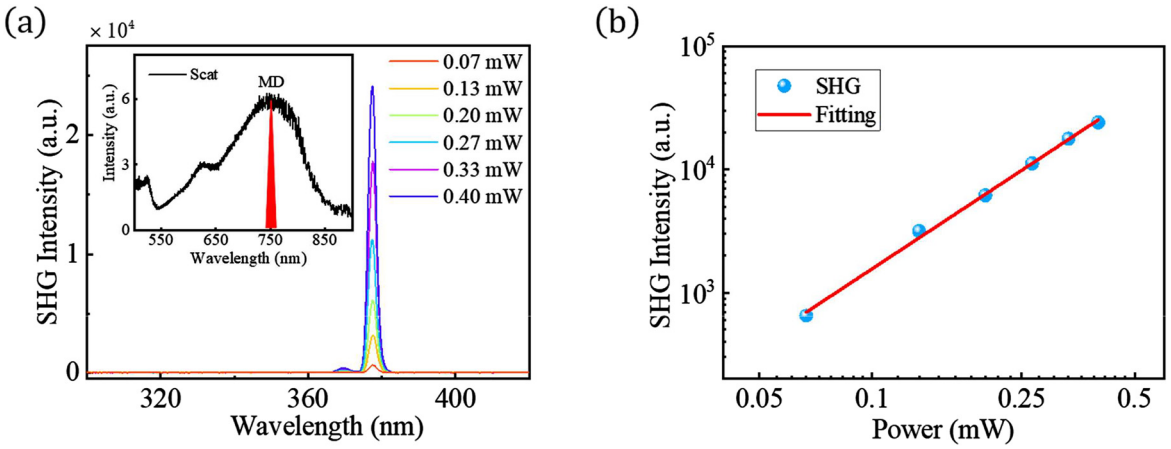

Figure 4: Power dependence of the SHG for LN nanosphere. (a) Measured spectra of SHG under different pump powers at MD resonance. The inset shows the spectral position of the pumping laser with respective of the MD mode. (b) Power dependence of SHG signals in (a), fitted by $P_{SHG} = mP^n_{pump}$. The exponent value obtained from the fitting is 2.0.

4 Conclusion

In summary, we fabricate the LN nanosphere supporting Mie resonances in visible via the laser ablation technique. Due to the MD Mie resonance, the LN nanosphere provides a considerable field enhancement for the generation of SHG in the UV range. The SHG reaches the maximum when pumping at the MD Mie resonance, resulting in a high SHG conversion efficiency of 4.45×10^{-8}. Our work provides a promising tool for enhancing nanoscale light–matter interactions in the UV regime. The Mie-resonant LN nanospheres could be further utilized to explore nonlinear nanophotonic devices such as frequency converters and quantum light sources via the nonlinear optical process, e.g., the parametric down-conversion process and four-wave mixing.

Author contribution: All the authors have accepted responsibility for the entire content of this submitted manuscript and approved submission.

Research funding: This research was supported by the National Key R&D Program of China (2018YFA0306100), the National Natural Science Foundation of China (62035017, 11874437).

Conflict of interest statement: The authors declare no conflicts of interest regarding this article.

References

[1] A. J. Goodman and W. A. Tisdale, "Enhancement of second-order nonlinear-optical signals by optical stimulation," *Phys. Rev. Lett.*, vol. 114, no. 18, p. 183902, 2015.

[2] X. Zhang, Q.-T. Cao, Z. Wang, et al., "Symmetry-breaking-induced nonlinear optics at a microcavity surface," *Nat. Photonics*, vol. 13, no. 1, pp. 21–24, 2019.

[3] U. Petzold, A. Büchel, and T. Halfmann, "Effects of laser polarization and interface orientation in harmonic generation microscopy," *Opt. Express*, vol. 20, no. 4, pp. 3654–3662, 2012.

[4] S. Kushwaha, M. Shakir, K. Maurya, A. Shah, M. Wahab, and G. Bhagavannarayana, "Remarkable enhancement in crystalline perfection, second harmonic generation efficiency, optical transparency, and laser damage threshold in potassium dihydrogen phosphate crystals by L-threonine doping," *J. Appl. Phys.*, vol. 108, no. 3, 2010, Art no. 033506.

[5] R. Su, M. Zhu, Z. Huang, B. Wang, and W. Wu, "Second harmonic generation efficiency affected by radiation force of a high-energy laser beam through stress within a mounted potassium dihydrogen phosphate crystal," *Opt. Eng.*, vol. 57, no. 1, 2018, Art no. 015106.

[6] S. G. Grechin, V. G. Dmitriev, V. A. Dyakov, and V. I. Pryalkin, "Temperature-independent phase matching for second-harmonic generation in a KTP crystal," *Quant. Electron.*, vol. 29, no. 1, p. 77, 1999.

[7] B. Y. Zel'dovich, Y. E. Kapitski, and A. Chudinov, "Interference between second harmonics generated into different KTP crystals," *Sov. J. Quant. Electron.*, vol. 20, no. 9, p. 1120, 1990.

[8] J. Chen, P. Han, and X.-C. Zhang, "Terahertz-field-induced second-harmonic generation in a beta barium borate crystal and its application in terahertz detection," *Appl. Phys. Lett.*, vol. 95, no. 1, 2009, Art no. 011118.

[9] P. Banks, M. Feit, and M. Perry, "High-intensity third-harmonic generation in beta barium borate through second-order and third-order susceptibilities," *Opt. Lett.*, vol. 24, no. 1, pp. 4–6, 1999.

[10] B. Corcoran, C. Monat, C. Grillet, et al., "Green light emission in silicon through slow-light enhanced third-harmonic generation in photonic-crystal waveguides," *Nat. Photonics*, vol. 3, no. 4, pp. 206–210, 2009.

[11] J. Wang, M. Clementi, M. Minkov, et al., "Doubly resonant second-harmonic generation of a vortex beam from a bound

state in the continuum,'' *Optica*, vol. 7, no. 9, pp. 1126–1132, 2020.
[12] X. Lu, G. Moille, A. Rao, D. A. Westly, and K. Srinivasan, ''Efficient photoinduced second-harmonic generation in silicon nitride photonics,'' *Nat. Photonics*, vol. 15, no. 2, pp. 1–6, 2020.
[13] X. Lu, Q. Li, D. A. Westly, et al., ''Chip-integrated visible–telecom entangled photon pair source for quantum communication,'' *Nat. Phys.*, vol. 15, no. 4, pp. 373–381, 2019.
[14] G. Grinblat, Y. Li, M. P. Nielsen, R. F. Oulton, and S. A. Maier, ''Degenerate four-wave mixing in a multiresonant germanium nanodisk,'' *ACS Photonics*, vol. 4, no. 9, pp. 2144–2149, 2017.
[15] K. Koshelev, S. Kruk, E. Melik-Gaykazyan, et al., ''Subwavelength dielectric resonators for nonlinear nanophotonics,'' *Science*, vol. 367, no. 6475, pp. 288–292, 2020.
[16] Y. Kivshar and A. Miroshnichenko, ''Meta-optics with Mie resonances,'' *Opt. Photon. News*, vol. 28, no. 1, pp. 24–31, 2017.
[17] S. Kruk and Y. Kivshar, ''Functional meta-optics and nanophotonics governed by Mie resonances,'' *ACS Photonics*, vol. 4, no. 11, pp. 2638–2649, 2017.
[18] P. A. Dmitriev, D. G. Baranov, V. A. Milichko, et al., ''Resonant Raman scattering from silicon nanoparticles enhanced by magnetic response,'' *Nanoscale*, vol. 8, no. 18, pp. 9721–9726, 2016.
[19] M. R. Shcherbakov, D. N. Neshev, B. Hopkins, et al., ''Enhanced third-harmonic generation in silicon nanoparticles driven by magnetic response,'' *Nano Lett.*, vol. 14, no. 11, pp. 6488–6492, 2014.
[20] E. V. Melik-Gaykazyan, M. R. Shcherbakov, A. S. Shorokhov, et al., ''Third-harmonic generation from Mie-type resonances of isolated all-dielectric nanoparticles,'' *Phil. Trans. Math. Phys. Eng. Sci.*, vol. 375, no. 2090, p. 20160281, 2017.
[21] H. Liu, C. Guo, G. Vampa, et al., ''Enhanced high-harmonic generation from an all-dielectric metasurface,'' *Nat. Phys.*, vol. 14, no. 10, pp. 1006–1010, 2018.
[22] G. Marino, A. S. Solntsev, L. Xu, et al., ''Spontaneous photon-pair generation from a dielectric nanoantenna,'' *Optica*, vol. 6, no. 11, pp. 1416–1422, 2019.
[23] T. Santiago-Cruz, A. Fedotova, V. Sultanov, et al., ''Photon pairs from resonant metasurfaces,'' *Nano Lett.*, vol. 10, pp. 4423–4429, 2021.
[24] A. Vaskin, J. Bohn, K. E. Chong, et al., ''Directional and spectral shaping of light emission with Mie-resonant silicon nanoantenna arrays,'' *ACS Photonics*, vol. 5, no. 4, pp. 1359–1364, 2018.
[25] S. Liu, A. Vaskin, S. Addamane, et al., ''Light-emitting metasurfaces: simultaneous control of spontaneous emission and far-field radiation,'' *Nano Lett.*, vol. 18, no. 11, pp. 6906–6914, 2018.
[26] S. T. Ha, Y. H. Fu, N. K. Emani, et al., ''Directional lasing in resonant semiconductor nanoantenna arrays,'' *Nat. Nanotechnol.*, vol. 13, no. 11, pp. 1042–1047, 2018.
[27] G. Grinblat, Y. Li, M. P. Nielsen, R. F. Oulton, and S. A. Maier, ''Efficient third harmonic generation and nonlinear subwavelength imaging at a higher-order anapole mode in a single germanium nanodisk,'' *ACS Nano*, vol. 11, no. 1, pp. 953–960, 2017.
[28] G. Grinblat, Y. Li, M. P. Nielsen, R. F. Oulton, and S. A. Maier, ''Enhanced third harmonic generation in single germanium nanodisks excited at the anapole mode,'' *Nano Lett.*, vol. 16, no. 7, pp. 4635–4640, 2016.
[29] R. Weis and T. Gaylord, ''Lithium niobate: summary of physical properties and crystal structure,'' *Appl. Phys. A*, vol. 37, no. 4, pp. 191–203, 1985.
[30] Y. Kong, F. Bo, W. Wang, et al., ''Recent progress in lithium niobate: optical damage, defect simulation, and on-chip devices,'' *Adv. Mater.*, vol. 32, no. 3, p. 1806452, 2020.
[31] M. J. Weber, *Handbook of Optical Materials*, vol. 19. Boca Raton, CRC Press, 2002.
[32] E. D. Palik, *Handbook of Optical Constants of Solids*, vol. 3. San Diego, Academic Press, 1998.
[33] F. Timpu, J. Sendra, C. Renaut, et al., ''Lithium niobate nanocubes as linear and nonlinear ultraviolet Mie resonators,'' *ACS Photonics*, vol. 6, no. 2, pp. 545–552, 2019.
[34] S. V. Makarov, M. I. Petrov, U. Zywietz, et al., ''Efficient second-harmonic generation in nanocrystalline silicon nanoparticles,'' *Nano Lett.*, vol. 17, no. 5, pp. 3047–3053, 2017.
[35] J. Xiang, S. Jiang, J. Chen, et al., ''Hot-electron intraband luminescence from GaAs nanospheres mediated by magnetic dipole resonances,'' *Nano Lett.*, vol. 17, no. 8, pp. 4853–4859, 2017.
[36] J. Xiang, J. Chen, S. Jiang, et al., ''Liquid gallium nanospheres emitting white light,'' *Laser Photon. Rev.*, vol. 13, no. 5, p. 1800214, 2019.
[37] F. Timpu, A. Sergeyev, N. R. Hendricks, and R. Grange, ''Second-harmonic enhancement with Mie resonances in perovskite nanoparticles,'' *ACS Photonics*, vol. 4, no. 1, pp. 76–84, 2017.
[38] E. A. Gurvitz, K. S. Ladutenko, P. A. Dergachev, A. B. Evlyukhin, A. E. Miroshnichenko, and A. S. Shalin, ''The high-order toroidal moments and anapole states in all-dielectric photonics,'' *Laser Photon. Rev.*, vol. 13, no. 5, p. 1800266, 2019.
[39] J. Ma, F. Xie, W. Chen, et al., ''Nonlinear lithium niobate metasurfaces for second harmonic generation,'' *Laser Photon. Rev.*, vol. 15, no. 5, p. 2000521, 2021.
[40] A. Fedotova, M. Younesi, J. Sautter, et al., ''Second-harmonic generation in resonant nonlinear metasurfaces based on lithium niobate,'' *Nano Lett.*, vol. 20, no. 12, pp. 8608–8614, 2020.
[41] Y. Li, Z. Huang, Z. Sui, et al., ''Optical anapole mode in nanostructured lithium niobate for enhancing second harmonic generation,'' *Nanophotonics*, vol. 9, no. 11, pp. 3575–3585, 2020.